



## Research paper

Adaptive fuzzy weighted C-mean image segmentation algorithm combining a new distance metric and prior entropy<sup>☆</sup>Sensen Song<sup>a,b</sup>, Zhenhong Jia<sup>a,\*</sup>, Fei Shi<sup>a</sup>, Junnan Wang<sup>a</sup>, Dongdong Ni<sup>a</sup><sup>a</sup> School of Computer Science and Technology, Key Laboratory of Signal Detection and Processing, Xinjiang Uygur Autonomous Region, Xinjiang University, Urumqi, 830046, Xinjiang, China<sup>b</sup> College of Mathematics and System Science, Xinjiang University, Urumqi, 830046, Xinjiang, China

## ARTICLE INFO

Dataset link: <https://www2.eecs.berkeley.edu/Research/Projects/CS/vision/grouping/resources.html>, <https://dags.stanford.edu/projects/secedataset.html>

**Keywords:**  
 FCM  
 Initialization settings  
 Distance metric  
 Fuzzy weight  
 Prior entropy  
 Image segmentation

## ABSTRACT

The fuzzy C-mean clustering algorithm (FCM) is effective in image segmentation. However, its sensitivity to initialization settings and the limitation of the Euclidean distance metric in measuring similarity lead to unsatisfactory image segmentation. To overcome these shortcomings, we propose an adaptive fuzzy weighted C-mean image segmentation algorithm that combines a new distance metric and prior entropy. This algorithm significantly contributes in three aspects. First, we employ an improved sparse subspace clustering (SSC) algorithm based on the superpixel image for initialization settings. This step aims to obtain the initial number of clusters and the membership matrix, ensuring the algorithm's convergence to the optimal solution. Second, to better capture differences between image regions, we introduce a novel distance metric that combines Euclidean and non-Euclidean distances. Simultaneously, the fuzzy weight is introduced to mitigate redundant feature interference, making the clustering result more reasonable. Finally, leveraging prior entropy – a maximum entropy under conditional constraints – we refine the algorithm's adaptability to unknown features, thereby improving clustering accuracy. Comparative experiments with several state-of-the-art algorithms validate the effectiveness and robustness of our proposed algorithm.

## 1. Introduction

FCM is one of the most frequently used clustering algorithms based on fuzzy theory in image segmentation (Bezdek et al., 1984; Nayak et al., 2015; Havens et al., 2012; Chen and Zhang, 2004), which is simple, efficient, and adaptable. Moreover, several reasons for the popularity of FCM in image segmentation are as follows: (1) FCM is simple in design and easy to implement, which can be derived from the objective function Eq. (1). Moreover, it transforms the image segmentation problem into an optimization problem (Zhang et al., 2019); (2) FCM always converges to a solution, so the derived fuzzy membership matrix is consistent, which ensures its robustness; (3) In practical applications, since the influence of multiple uncertainties, such as image degradation and noise interference, Hard C-means (HCM) method is difficult to accurately classify different pixels or regions into the categories they belong to, and their classification is accompanied by uncertainty. Moreover, the fuzzy theory is a powerful tool for describing uncertainty (Gou et al., 2017; Amane et al., 2023; Bhadane et al., 2022; Surono et al., 2023). Thus FCM replaces the independence

between each category with a concept of membership, overcoming the deficiency of HCM to classify pixels in a one-size-fits-all way.

Although FCM has numerous advantages over other clustering algorithms, it also comes with inherent drawbacks, mainly manifested in the following aspects: (1) The structure of FCM makes it vulnerable to initialization, meaning it is sensitive to initial values and tends to converge to local minima, making it challenging to achieve a globally optimal solution (Sun et al., 2004). Consequently, the choice of initialization greatly influences the objective function's optimal solution. According to Lyapunov stability theory, the fuzzy clustering algorithm is asymptotically stable in the vicinity of cluster centers. However, this stability is not consistently achieved across a broad range of cluster centers (Nie et al., 2007), relying heavily on the accuracy of the initial cluster center and membership estimates. (2) The commonly used Euclidean distance in FCM struggles to accurately measure the similarity between features in a high-dimensional feature space (Spruyt, 2014). Furthermore, due to the high dimensionality of image features employed in image clustering segmentation, it frequently results in unsatisfactory segmentation outcomes.

<sup>☆</sup> This work was supported by the National Natural Science Foundation of China (No. U1803261 and 62261053), the Natural Science Foundation of XinJiang under Grant 2022D01C58, and Scientific Research Plan of Universities in Xinjiang Uygur Autonomous Region under Grant XJEDU2019Y006.

\* Corresponding author.

E-mail address: [jzh@xju.edu.cn](mailto:jzh@xju.edu.cn) (Z. Jia).

To tackle this initialization challenge, researchers have proposed numerous approaches. Primarily, initialization settings involve establishing the cluster number and the membership matrix. The initialization of the cluster number often relies on empirical values or the number of categories obtained through other algorithms based on image features. For example, ENFCM (Szilagyi et al., 2003), FGFCM (Cai et al., 2007), FLICM (Krinidis and Chatzis, 2010), FRFCM (Lei et al., 2018a), KWFLICM (Gong et al., 2012), DSFCM (Zhang et al., 2018), SFFCM (Lei et al., 2018b), etc., whose cluster numbers are generally set empirically; while such as CGFFCM (Oskouei et al., 2021), AFCF (Lei et al., 2019), and ICAFKM (Emami and Derakhshan, 2015) adopt some specific algorithms to obtain the number of clusters. In addition, for the initialization of the membership matrix, some algorithms use random initialization, such as ENFCM, FGFCM, FLICM, FRFCM, KWFLICM, DSFCM, and SFFCM. And FCM\_S (Ahmed et al., 2002), FCM\_SICM (Wang et al., 2020), AFCF, RSSFCA (Jia et al., 2020), ICAFKM, CGFFCM and other algorithms employ FCM algorithm, ICA algorithm or directly set a certain initial value matrix. It is evident that while random initialization might increase the likelihood of obtaining the optimal solution to some extent, it also introduces random variations in the segmentation results. Initialization settings derived from certain specific algorithms converge either to local minima or global minima, yielding stable segmentation outcomes. However, the aforementioned algorithms did not utilize the same approach to obtain the number of clusters and the membership matrix, resulting in a lack of correlation between them.

To address the limitations of the Euclidean distance metric in expressing similarity effectively, several non-Euclidean-based distance metric methods have been proposed. For instance, KWFLICM incorporates a kernel distance metric into its objective function, transforming the nonlinear problem from a low-dimensional input space into a linear problem in a high-dimensional input space, thereby improving image segmentation performance. However, this improvement comes with increased computational complexity. AFCF proposes a prior entropy-based fuzzy clustering algorithm that utilizes covariance analysis and Markov random fields to measure similarity between different superpixel areas. Yet, its performance is constrained by the superpixel feature. RSSCA defines feature similarity using the logarithm of the Gaussian density function, but it is sensitive to parameter settings. These methods enhance clustering accuracy by introducing non-Euclidean distances to calculate similarity between image features and clustering centers. Additionally, the limitation of the Euclidean distance can be tackled by employing a fuzzy weighting method that considers the varying importance (weight) of individual features regarding the clustering centers. Wang et al. proposed a feature-weighted learning method (Wang et al., 2004), called WFCM, to improve the performance of FCM for clustering. In Yang and Nataliani (2017), Yang et al. presented a new method, the feature-weighted entropy FCM objective function, aimed at eliminating irrelevant features with small weights. This method automatically calculates individual feature weights while reducing redundant feature components, enabling clustering of high-dimensional features. In 2016, Zhou et al. introduced the maximum entropy-adjusted weighted FCM (EWFCM) (Zhou et al., 2016). This method is based on a regularization technique involving local feature weight entropy, achieved by constructing a new objective function to determine the optimal feature weights. CGFFCM also improves the accuracy of image clustering by using feature weights. However, improper weight assignment can potentially lead to performance degradation. In addition, Guo et al. proposed a soft subspace clustering algorithm that addresses the correlation among data dimensions for clustering high-dimensional features (Guo et al., 2022). This method incorporates a novel dimensional affinity regularization term into the objective function, highlighting feature subspace-related dimensions crucial for cluster formation. FSC\_LNML (Wei et al., 2022) adaptively constrains the local variance and non-local information in the original image using the absolute intensity difference of local variance and non-local information and its inverse. It introduces the

concept of subspace to dynamically assign suitable weights to each image dimension, enhancing color image segmentation performance. While fuzzy subspace clustering algorithm solves the problem of inflexible dimension selection of subspace dimensions by assigning different weights to each dimension through density sparsity. However, it is difficult to define an accurate distance metric function and the complexity of the algorithm increases dramatically.

To solve the issues related to initialization settings and the inadequacy of feature similarity expressed by the Euclidean distance, we propose an adaptive fuzzy weighted C-mean image segmentation algorithm that combines a new distance metric and prior entropy. First, the input image is converted into a superpixel image to reduce the running time. Based on the superpixel image, we employ the regularization term of the  $l_1$ -norm SSC (Elhamifar and Vidal, 2013; Li et al., 2017; Zhang et al., 2013) to represent the correlation between image regions. Moreover, a reasonable number of clusters and initial values of the membership matrix can be obtained, thus improving the robustness and convergence speed of the proposed method. Second, to overcome the shortage of Euclidean distance, we improve its performance in two ways. One is to add a multivariate Gaussian distribution to compensate for the Euclidean distance and increase the feature distance measure of multidimensional variables. The other is introducing fuzzy weights to mitigate the impact of redundant features on clustering, resulting in more rational clustering outcomes. Finally, the fuzzy weighted C-mean algorithm improves the segmentation accuracy of images by exploiting the ability of prior entropy for different image data.

Our proposed algorithm presents three main advantages over previous work as follows:

1. To secure reasonable initialization values ensuring convergence to the optimal solution, we present an initialization algorithm based on SSC. This method derives both the number of clusters and the membership matrix for initialization settings, significantly enhancing the robustness of our proposed algorithm compared to other existing FCM algorithms.
2. Euclidean distance does not serve as an optimal measure of similarity between multidimensional features. To address this, we construct a distance metric by combining both Euclidean and non-Euclidean distances, as well as introduce fuzzy weights to achieve accurate clustering of features.

The rest of this paper is organized as follows. In Section 2, we illustrate the preliminary theory. In Section 3, we propose our methodology and analyze its superiority. The experimental results and analysis are in Section 4. Finally, we present our conclusion in Section 5.

## 2. Preliminary theory

In this section, we review the relevant algorithms and theories involved in our proposed algorithm.

### 2.1. FCM algorithm

The FCM algorithm was first proposed by Dunn (1973) and later extended by Bezdek (2013). It is an unsupervised clustering method that does not require human intervention during the implementation. It is also an iterative clustering method that assigns data to appropriate clustering centers by iterating the membership and clustering centers. When the errors of the iterations satisfy the set conditions, the memberships of each data with the clustering centers are compared to obtain the clustering results.

$$J_m(U, V) = \sum_{i=1}^c \sum_{j=1}^n u_{ij}^m \|x_j - v_i\|^2 \quad (1)$$

where  $c$  is the number of clusters,  $n$  is the total number of data.  $U = \{u_{ij}^m\}$  is the fuzzy membership of  $x_j$  with respect to the clustering center

$V = \{v_i\}$ ,  $0 \leq u_{ij} \leq 1$ , and  $\sum_{i=1}^c u_{ij} = 1$ .  $m$  is the fuzzification index of membership matrix  $U$ .  $\|\cdot\|$  denotes the Euclidean norm.

The solution of Eq. (1) can be obtained by the following iterative procedure.

Step 1: Set the number of clusters  $n$ , the fuzzy factor  $m$ , the error  $\epsilon$ , and the maximum number of iterations  $T_{max}$ .

Step 2: Initialize the membership matrix  $U^{t=0}$ .

Step 3: Calculate the clustering centers  $V^t$ ,

$$v_i^t = \frac{\sum_{j=1}^n (u_{ij}^t)^m x_j}{\sum_{j=1}^n (u_{ij}^t)^m} \quad (2)$$

Step 4: Calculate the membership matrix  $U^{t+1}$ ,

$$u_i^t = \frac{1}{\sum_{i=1}^c \left( \frac{\|x_j - v_i^t\|}{\|x_j - v_i^t\|} \right)^{2/m-1}} \quad (3)$$

Step 5: If  $J^t - J^{t+1} < \epsilon$  or  $t > T_{max}$ , then stop iteration, otherwise return to Step 3 and continue the loop.

## 2.2. SSC model

In subspace clustering, it is assumed that each sample can be represented by a linear combination of other samples, i.e.,  $X = XZ$ , and  $Z$  is the coefficient matrix, indicating the samples' degree of similarity. Generally, the SSC model can be uniformly described as the following optimization problem (Hu et al., 2014):

$$\begin{aligned} \min_{Z,E} J(Z) &= \Omega(Z) + \lambda\phi(E) \\ \text{s.t. } X &= XZ + E, Z \in R^{N \times N} \end{aligned} \quad (4)$$

where  $R^{N \times N}$  is the constraint set of the coefficient matrix  $Z$ .  $\Omega(Z)$  is the regularization term.  $E$  denotes the noises, corrupts, or outliers.  $\phi(E)$  is the data term, which portrays the degree of approximation between the representation  $XZ$  of the data and the data  $X$ .

## 2.3. Fuzzy weighted C-mean algorithm

The FCM algorithm treats image features of all dimensions equally, but the influence of features between different dimensions may not be equal in the clustering process. We can improve the accuracy of image clustering by assigning appropriate weights to each image feature. This approach helps overcome the drawbacks caused by the Euclidean distance metric. Moreover, there are two ways available. One way focuses on feature weights. Wang et al. proposed a feature-weighted learning method named WFCM, enhancing the performance of FCM. The other way operates from a subspace perspective. Gan et al. (2006) introduced the fuzzy subspace clustering (FSC) algorithm, which clusters high-dimensional datasets by assigning suitable weights to different dimensions' data. The objective function of WFCM can be expressed as

$$J_m(U, W, V) = \sum_{i=1}^c \sum_{j=1}^n \sum_{d=1}^k u_{id}^m w_{id}^\tau \|x_{ij} - v_{id}\|^2 \quad (5)$$

where  $\sum_{d=1}^k w_{id} = 1$ ,  $\sum_{i=1}^c u_{ij} = 1$ .  $d$  is the data dimension,  $\tau$  is the fuzzy weighting factor, and is always set  $\tau > 1$ .  $w$  is a feature weight by minimizing an evaluation function that follows from the procedure of Yeung and Wang (2002).

## 2.4. Maximum entropy principle

The maximum entropy principle (Friedman and Shimony, 1971) was proposed by E.T. Jaynes in 1957, which holds that under the condition of limited knowledge, it is recommended to select the probability distribution that conforms to such knowledge but with the maximum

entropy (Gou et al., 2017; Bajgiran et al., 2021; Eskenazis et al., 2018). In the FCM algorithm, if the entropy of the membership  $u_{ij}$  is the maximized, the assignment of feature vectors into clusters is characterized by maximum uncertainty or minimum selectivity (Karayiannis, 1994). In the maximum uncertainty or minimum selectivity stage, the process of the maximum entropy clustering algorithm is as follows: first, the maximum entropy is represented as

$$E(U) = - \sum_{i=1}^c \sum_{j=1}^n u_{ij} \ln u_{ij} \quad (6)$$

Second, the distance between the feature vector and the clustering center is known to be

$$D(U) = \sum_{i=1}^c \sum_{j=1}^n u_{ij} \|x_j - v_i\|^2 \quad (7)$$

Finally, its objective function (Karayiannis, 1994) is:

$$J(U, E) = (1 - \alpha) \sum_{i=1}^c \sum_{j=1}^n u_{ij} \|x_j - v_i\|^2 + \alpha \sum_{i=1}^c \sum_{j=1}^n u_{ij} \ln u_{ij} \quad (8)$$

where the parameter  $\alpha$  gradually decreases from close to 1 and gradually approaches zero. It assigns a relatively high role to entropy maximization in the initial clustering stage. As  $\alpha$  decreases, the influence of the entropy term decreases, and the minimization of the error between the feature vector and the prototype plays an increasingly important role. When  $\alpha$  approaches zero, the influence of the entropy term in Eq. (8) almost disappears. In conclusion,  $\alpha$  controls the transition from soft to hard decision-making in the clustering process.

## 3. The proposed algorithm

Building upon the algorithms and theories discussed in the previous section, we propose an adaptive fuzzy weight C-mean image segmentation algorithm combining a new distance measure and a prior entropy. The structural framework of the proposed algorithm is shown in Fig. 1 and the following are the main components of the proposed algorithm in this paper: (1) Initialization settings: These settings are crucial for achieving adaptive clustering based on the image content and ensuring convergence towards the optimal solution. (2) Distance metric: While the Euclidean distance is simple, intuitive, and performs well in low-dimensional data clustering, it is less effective in high-dimensional data clustering. Hence, we integrate both Euclidean and non-Euclidean distances to enhance clustering outcomes. (3) Fuzzy weights: FCM treats image features in all dimensions equally, but the impact of features may vary between different dimensions during clustering. Assigning appropriate weights to each dimension helps overcome the drawbacks of Euclidean distance, thereby enhancing image clustering accuracy. (4) A prior entropy: This factor reduces parameter influence and enhances the algorithm's processing capability for diverse image data, thus improving image segmentation accuracy. (5) Iterative computation: Through iterative computation of the objective function, we derive the optimal solution. (6) Convergence analysis: We demonstrate the algorithm's convergence, affirming that the objective function attains a local minimum, securing the optimal solution.

### 3.1. Initialization settings

To achieve adaptive initialization of the cluster number and the membership matrix based on the image content, we introduce a Gaussian-constrained SSC algorithm. This algorithm primarily involves two steps. First, we employ an enhanced superpixel algorithm to generate superpixel images. Second, we utilize the Gaussian regularization term to constrain the SSC model, yielding the optimized sparse coefficient matrix. This matrix serves as the membership matrix at this stage, and its rank determines the number of clusters.

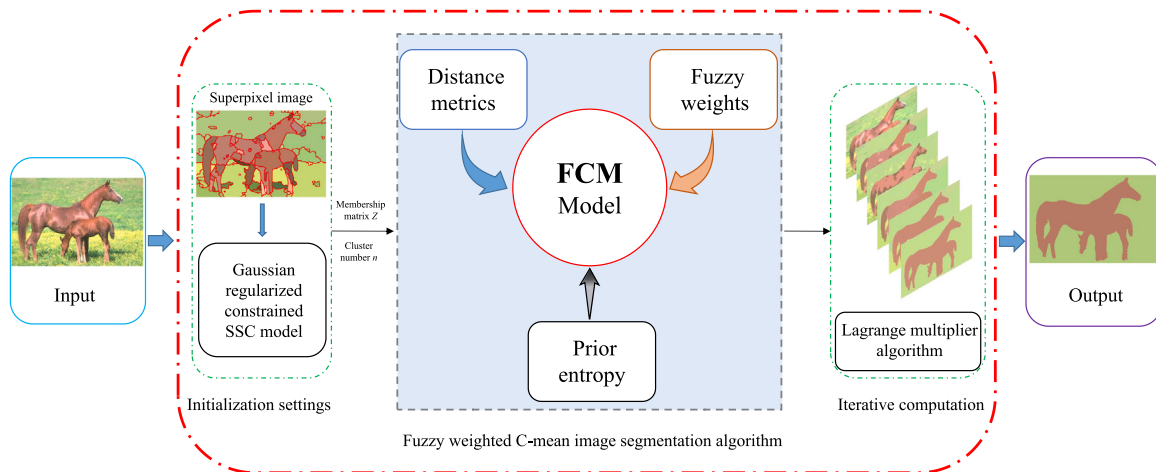


Fig. 1. The structural framework of the proposed algorithm.

### 3.1.1. Superpixel image

Superpixels (Achanta et al., 2012; Shen et al., 2016; Li and Chen, 2015; Ban et al., 2018; Lei et al., 2018b) are irregular blocks of pixels with somewhat visual significance composed of neighboring pixels with similar texture, color, brightness, and other features. They leverage feature similarities among pixels to create these groupings. Additionally, they condense numerous pixels into a smaller set of superpixels, effectively representing image features and significantly reducing image processing complexity. In practical applications, much of the image processing involves matrix operations. Consequently, working with pixel-based color images often incurs lengthy operation times. However, converting an image into a superpixel format can notably decrease computational requirements.

Take Fig. 2 as an example, the size of its original image is  $321 \times 481 \times 3$ , and the number of its pixels per channel is 154401, so there is no doubt that the size of its similarity matrix is  $154401 \times 154401$ , which produces the data with an order of magnitude of  $10^{10}$ . If the original image is converted to a superpixel image, the pixel number is reduced to a few hundred, and its similarity matrix order of magnitude is  $10^4$ . Therefore, the superpixel processing reduces the data amount significantly and provides the local similarity information of the image. Fig. 2 shows the color distribution corresponding to the image in Fig. 2. In Fig. 3, we can find that the superpixel image is easier to cluster by comparing the input with the superpixel image.

In SFFCM and AFCF, the effectiveness of superpixel preprocessing for subsequent processing has been demonstrated. This preprocessing step enhances the efficiency of image processing by incorporating local information from image pixels. Superpixels are small regions formed by adjacent pixel points with similar features like color, luminance, and texture. However, the quality of their outcomes depends on gradient images, and preserving edges is crucial for achieving desirable results. To obtain better results, we have refined the superpixel algorithm of MMGR-WT by incorporating edges from Dollár and Zitnick (2014) instead of relying solely on those from SFFCM. This enhancement is rooted in Dollár and Zitnick (2014) addressing the prediction of local edge masks within a structured learning framework applied to a stochastic decision forest. This approach enables the learning of precise and computationally efficient edge detectors by leveraging the inherent structure found in local image blocks. As illustrated in Fig. 2, our improved superpixel image exhibits finer details compared to the MMGR superpixel image, ensuring the accuracy of subsequent processing steps.

### 3.1.2. Gaussian regularized constrained SSC model

The existing  $\ell_1$ -norm SSC model is not strong in expressing the correlation between image regions, leading to its unsatisfactory accuracy

in natural image segmentation. In this paper, we propose a Gaussian regularization term that allows the data to be linearly represented by the most similar data possible. Specifically, we take the probability density function of the Gaussian distribution of the sparse coefficient matrix  $Z$  as the Gaussian regularization term, that is

$$Z_G(Z | M, \Sigma_n) = \frac{1}{(2\pi)^{N/2} \det^{1/2}(\Sigma_n)} \exp\left(-\frac{1}{2}(Z - \mu_n)^T \Sigma_n^{-1} (Z - \mu_n)\right) \quad (9)$$

where  $Z = \{z_1, z_2, \dots, z_N\}$ ,  $M = \{\mu_n\}_{1 \leq n \leq N} \in R^{N \times N}$  is the mean matrix of  $Z$ ,  $\Sigma_n$  is the covariance matrix of  $\{z_n\}_{1 \leq n \leq N}$ .  $\{z_n\}_{1 \leq n \leq N}$  and  $\{\mu_n\}_{1 \leq n \leq N}$  are  $N$ -dimensional vectors.

Drawing inspiration from the varying Gaussian distributions that characterize features in an image, we make a similar assumption regarding the relational data within the coefficient matrix. We hypothesize that these data follow distinct Gaussian distributions and posit that adjusting the mean values in the coefficient matrix can strengthen the associations between features. When  $M$  is the mean of the coefficient matrix  $Z$ ,  $Z_G(Z | M, \Sigma_n)$  is  $Z_G^1(Z | M, \Sigma_n)$ , then  $Z_G^1$  results in a stronger correlation of the data with relatively large differentiation following the nature of Gaussian function, which could be beneficial for image clustering, but it sometimes leads to the opposite result. Therefore, we also set  $M = \mathbf{1}$ ,  $\mathbf{1}$  is a matrix with all 1, then  $Z_G(Z | M, \Sigma_n)$  is  $Z_G^2(Z | M, \Sigma_n)$ , which enhances the differentiation within the data. By analyzing the aforementioned way, we can fine-tune the coefficients of  $Z_G^1 = Z_G^1(Z | M, \Sigma_n)$  and  $Z_G^2 = Z_G^2(Z | M, \Sigma_n)$ , thus enhancing the correlation representation of SSC.

To do so, we derive a Gaussian regularization constrained SSC for image segmentation as follows:

$$\begin{aligned} & \min_{Z, A, E} \|Z\|_1 + \lambda_1 \|A \odot Z_G^1\|_F^2 + \lambda_2 \|A \odot Z_G^2\|_F^2 + \delta \|E\|_1 \\ & \text{s.t. } X = ZX + E, A = Z - \text{diag}(Z), \end{aligned} \quad (10)$$

where  $\lambda_1 > 0$ ,  $\lambda_2 > 0$ , and  $\delta > 0$ . The  $\odot$  represents element-wise multiplication. We obtain the sparse coefficient matrix  $Z$  by solving Eq. (10) using the Alternating Direction Method of Multipliers (ADMM) (Boyd et al., 2010). Here, the sparse coefficient matrix  $Z$  characterizes the correlation between image features and associates each superpixel region. Therefore, we use the solved matrix  $Z$  as the membership matrix, facilitating better convergence of the clustering process towards the optimal solution. Moreover, considering the sparsity of matrix  $Z$ , its rank is evidently less than or equal to the dimensionality of the matrix. Thus, its rank serves as the determinant for the number of clusters. Moreover, to obtain a more reasonable cluster number, the following strategy is used to optimize the membership matrix  $Z$ ,

$$Z = Z(Z_{e(Z-\text{mean}(Z))<1} = 0) \quad (11)$$

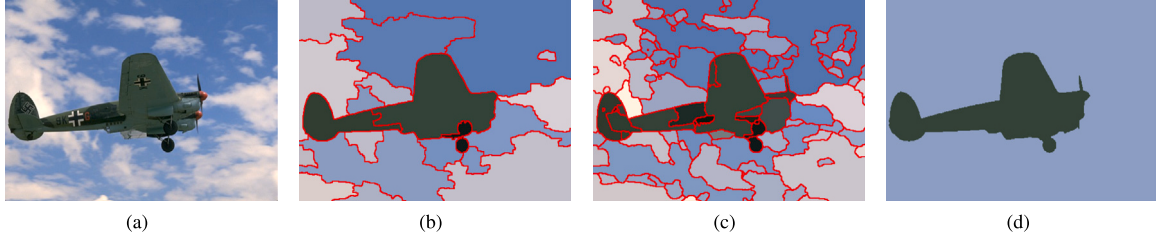


**Fig. 2.** Superpixel image. (a) Original image “3063”, (b) Superpixel generated by the SFFCM algorithm, (c) Our superpixel image, (d) Groundtruth.

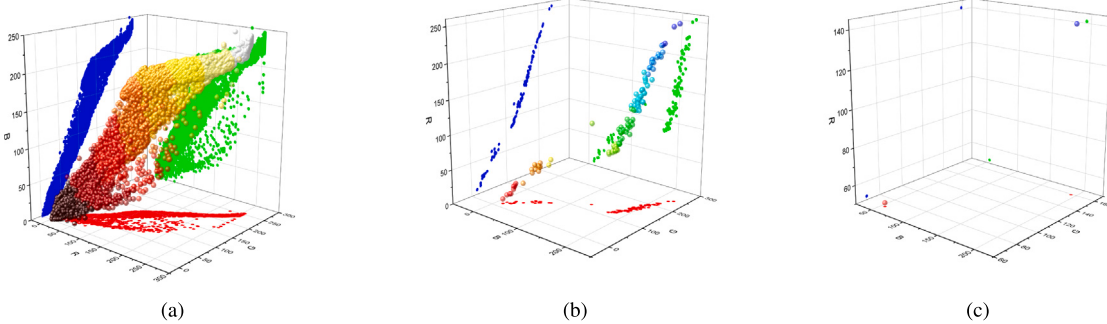


**Fig. 3.** Spatial distribution of color features. (a) The color space distribution with respect to a in Fig. 2, (b) The color space distribution with respect to c in Fig. 2, (c) The color space distribution with respect to d in Fig. 2.

Specifically, features with low relevance are assigned a value of 0. Multiple experiments indicate that the optimal performance for image clustering results occurs when the number of clusters matches the rank of matrix  $Z$ , determined by cycling the aforementioned Eq. (11) three times, denoted as  $n = \text{rank}(Z)$ .

### 3.2. A distance metric combining Euclidean and non-Euclidean distances

Previously, we discussed the advantages and limitations of the Euclidean distance metric. While Euclidean distance is straightforward and effective for clustering low-dimensional data, its performance diminishes in high-dimensional data. In high-accuracy segmentation, a single image feature may not suffice, necessitating the involvement of multidimensional image features in the clustering process. Consequently, the Euclidean distance struggles to adequately capture the correlation or differences among these features.

Researchers have proposed various methods based on alternative non-Euclidean distance measures to address this challenge. For instance, KWFLICM utilized a Gaussian kernel function distance, mapping two-dimensional data to a higher-dimensional space where nonlinear relationships become linearly separable. RCSSA and AFCF characterized feature similarity using multidimensional Gaussian distributions. To achieve better clustering of images, we propose a distance measure that combines Euclidean and non-Euclidean distance with the following equation:

$$J_m(U, V) = \sum_{i=1}^c \sum_{j=1}^n u_{ij}^m (\|x_j - v_i\|^2 + \Phi(x_j | v_i, \Sigma_i)) \quad (12)$$

where  $\Phi(x_j | v_i, \Sigma_i) = -\ln \rho(x_j | v_i, \Sigma_i)$  denotes the multivariate Gaussian distribution, which is used here as a non-Euclidean distance metric. Also,  $\rho$  is the Gaussian density function,

$$\rho(x_j | v_i, \Sigma_i) = \frac{1}{2\pi^{D/2} |\Sigma_i|^{1/2}} \exp(-\frac{1}{2} (x_j - v_i)^T \Sigma_i^{-1} (x_j - v_i)) \quad (13)$$

where  $D$  represents the dimensionality of the image features and  $\Sigma_i$  denotes the covariance matrix describing the intra-class distribution of class  $i$ . We can obtain

$$\Phi(x_j | v_i, \Sigma_i) = \frac{1}{2} ((x_j - v_i)^T \Sigma_i^{-1} (x_j - v_i) + \ln |\Sigma_i| + D \ln(2\pi)). \quad (14)$$

### 3.3. Fuzzy weights

To further overcome the drawbacks brought by Euclidean distance, or to supplement the above distance metric, which makes the image clustering better. We introduce fuzzy weights to improve the image clustering accuracy by assigning appropriate weights to each feature and controlling its different correlations to reduce the interference of irrelevant or redundant features. Then our new objective function is obtained according to Eq. (5),

$$J_m(U, W, V) = \sum_{i=1}^c \sum_{j=1}^n \sum_{d=1}^k u_{ij}^m w_{id}^\tau (\|x_j - v_i\|^2 + \Phi(x_j | v_i, \Sigma_i)) + \sum_{i=1}^c \sum_{d=1}^k w_{id}^\tau \quad (15)$$

where  $\sum_{d=1}^k w_{id} = 1$ ,  $\sum_{i=1}^c u_{ij} = 1$ .

### 3.4. A prior entropy

Eq. (15) shows that it involves relatively more constraints or variables, which requires us to adjust the adaptability to different image features and the degree of fitting to image pixels. Moreover, the maximum entropy method can solve the conditional constraint problem, so we propose to use the prior entropy of the membership matrix to make the clustering more reasonable and accurate. Based on Eq. (8), we present our final objective function as follows:

$$J(U, W, V) = \sum_{i=1}^c \sum_{j=1}^n \sum_{d=1}^k u_{ij} w_{id}^\tau (\|x_j - v_i\|^2 + \Phi(x_j | v_i, \Sigma_i)) + \alpha \sum_{i=1}^c \sum_{d=1}^k w_{id}^\tau + \gamma \sum_{i=1}^c \sum_{j=1}^n u_{ij} \ln u_{ij} \quad (16)$$

where  $\sum_{d=1}^k w_{id} = 1$ ,  $\sum_{i=1}^c u_{ij} = 1$ .  $\alpha$  and  $\gamma$  are clustering adjustment factors.

### 3.5. Iterative computation

According to the conditions of Eq. (16), the Lagrange multiplier algorithm is used to solve the optimal solution, then we have

$$\begin{aligned} J(U, W, V) = & \sum_{i=1}^c \sum_{j=1}^n \sum_{d=1}^k u_{ij} w_{id}^\tau (\|x_{jd} - v_{id}\|^2 + \Phi(x_{jd} | v_{id}, \Sigma_{id})) \\ & + \alpha \sum_{i=1}^c \sum_{d=1}^k w_{id}^\tau + \gamma \sum_{i=1}^c \sum_{j=1}^n u_{ij} \ln u_{ij} \\ & - \sum_{j=1}^n \lambda_1^1 (\sum_{i=1}^c u_{ij} - 1) - \sum_{i=1}^c \lambda_2^2 (\sum_{d=1}^k w_{id} - 1) \end{aligned} \quad (17)$$

where  $\lambda_1 = \sum_{j=1}^n \lambda_1^1$  and  $\lambda_2 = \sum_{i=1}^c \lambda_2^2$  are Lagrange multipliers.

First, we compute the partial derivative of  $u_{ij}$ ,

$$\begin{aligned} \frac{\partial J}{\partial u_{ij}} = & \sum_{d=1}^k w_{id}^\tau (\|x_{jd} - v_{id}\|^2 + \Phi(x_{jd} | v_{id}, \Sigma_{id})) + \gamma (\ln u_{ij} + 1) - \lambda_1 \\ \Rightarrow & \sum_{d=1}^k w_{id}^\tau (\|x_{jd} - v_{id}\|^2 + \Phi(x_{jd} | v_{id}, \Sigma_{id})) + \gamma (\ln u_{ij} + 1) - \lambda_1 = 0 \\ \Rightarrow \gamma (\ln u_{ij} + 1) = & \lambda_1 - \sum_{d=1}^k w_{id}^\tau (\|x_{jd} - v_{id}\|^2 + \Phi(x_{jd} | v_{id}, \Sigma_{id})) \\ \Rightarrow \ln u_{ij} = & \frac{1}{\gamma} (\lambda_1 - \sum_{d=1}^k w_{id}^\tau (\|x_{jd} - v_{id}\|^2 + \Phi(x_{jd} | v_{id}, \Sigma_{id})) - \gamma) \\ \Rightarrow u_{ij} = & \exp(\frac{1}{\gamma} (\lambda_1 - \sum_{d=1}^k w_{id}^\tau (\|x_{jd} - v_{id}\|^2 + \Phi(x_{jd} | v_{id}, \Sigma_{id})) - \gamma)) \end{aligned} \quad (18)$$

According to  $\sum_{i=1}^c u_{ij} = 1$ , then we can obtain

$$\begin{aligned} \sum_{i=1}^c u_{ij} = & \sum_{i=1}^c \exp(\frac{1}{\gamma} (\lambda_1 - \sum_{d=1}^k w_{id}^\tau (\|x_{jd} - v_{id}\|^2 + \Phi(x_{jd} | v_{id}, \Sigma_{id})) - \gamma)) \\ \Rightarrow & \sum_{i=1}^c \exp(\frac{1}{\gamma} (\lambda_1 - \sum_{d=1}^k w_{id}^\tau (\|x_{jd} - v_{id}\|^2 + \Phi(x_{jd} | v_{id}, \Sigma_{id})) - \gamma)) = 1 \\ \Rightarrow & \sum_{i=1}^c \exp(-\frac{1}{\gamma} (\sum_{d=1}^k w_{id}^\tau (\|x_{jd} - v_{id}\|^2 + \Phi(x_{jd} | v_{id}, \Sigma_{id})))) \\ = & \exp(\frac{1}{\gamma} (\gamma - \lambda_1)) \end{aligned} \quad (19)$$

The solution of  $\frac{\partial J}{\partial u_{ij}}$  yields

$$u_{ij} = \frac{\exp(-\frac{1}{\gamma} (\sum_{d=1}^k w_{id}^\tau (\|x_{jd} - v_{id}\|^2 + \Phi(x_{jd} | v_{id}, \Sigma_{id}))))}{\sum_{i=1}^c \exp(-\frac{1}{\gamma} (\sum_{d=1}^k w_{id}^\tau (\|x_{jd} - v_{id}\|^2 + \Phi(x_{jd} | v_{id}, \Sigma_{id}))))} \quad (20)$$

Second, by computing  $\frac{\partial J}{\partial v_{id}}$ , we have

$$\begin{aligned} \frac{\partial J}{\partial v_{id}} = & -\sum_{j=1}^n u_{ij} w_{id}^\tau ((x_{jd} - v_{id}) + \Sigma_{id}^{-1}(x_{jd} - v_{id})) \\ \Rightarrow & \sum_{j=1}^n u_{ij} w_{id}^\tau ((x_{jd} - v_{id}) + \Sigma_{id}^{-1}(x_{jd} - v_{id})) = 0 \\ \Rightarrow v_{id} = & \frac{\sum_{j=1}^n u_{ij} w_{id}^\tau (1 + \Sigma_{id}^{-1}) x_{jd}}{\sum_{j=1}^n u_{ij} w_{id}^\tau (1 + \Sigma_{id}^{-1})} \end{aligned} \quad (21)$$

Third, since the covariance matrix  $\Sigma_{id}$  changes with Eqs. (20) and (21), it is also necessary to calculate the partial derivatives of the

covariance matrix  $\Sigma_{id}$ , and

$$\begin{aligned} \frac{\partial J}{\partial \Sigma_{id}} = & \sum_{i=1}^c \sum_{j=1}^n \sum_{d=1}^k u_{ij} w_{id}^\tau \left( \frac{\partial \Phi(x_{jd} | v_{id}, \Sigma_{id})}{\partial \Sigma_{id}} \right) \\ \Rightarrow & \sum_{i=1}^c \sum_{j=1}^n \sum_{d=1}^k u_{ij} w_{id}^\tau \left( \frac{\partial \Phi(x_{jd} | v_{id}, \Sigma_{id})}{\partial \Sigma_{id}} \right) = 0 \\ \Rightarrow & \sum_{i=1}^c \sum_{j=1}^n \sum_{d=1}^k u_{ij} w_{id}^\tau \\ & \times \left( \frac{\partial \frac{1}{2} ((x_{jd} - v_{id})^T \Sigma_{id}^{-1} (x_{jd} - v_{id}) + \ln |\Sigma_{id}| + D \ln(2\pi))}{\partial \Sigma_{id}} \right) = 0 \\ \Rightarrow & \sum_{i=1}^c \sum_{j=1}^n \sum_{d=1}^k u_{ij} w_{id}^\tau \left( -\frac{1}{2} ((x_{jd} - v_{id})^T \Sigma_{id}^{-2} (x_{jd} - v_{id}) + \Sigma_{id}^{-1}) \right) = 0 \\ \Rightarrow & \Sigma_{id} = \frac{\sum_{i=1}^c \sum_{j=1}^n u_{ij} w_{id}^\tau \left( \frac{1}{2} (x_{jd} - v_{id})^T (x_{jd} - v_{id}) \right)}{\sum_{i=1}^c \sum_{j=1}^n u_{ij} w_{id}^\tau} \end{aligned} \quad (22)$$

Four, similarly, we compute  $\frac{\partial J}{\partial w_{id}}$ ,

$$\begin{aligned} \frac{\partial J}{\partial w_{id}} = & \sum_{j=1}^n \tau u_{ij} w_{id}^{\tau-1} (\|x_{jd} - v_{id}\|^2 + \Phi(x_{jd} | v_{id}, \Sigma_{id})) + \alpha \tau w_{id}^{\tau-1} - \lambda_2 \\ \Rightarrow & \sum_{j=1}^n \tau u_{ij} w_{id}^{\tau-1} (\|x_{jd} - v_{id}\|^2 + \Phi(x_{jd} | v_{id}, \Sigma_{id})) + \alpha \tau w_{id}^{\tau-1} - \lambda_2 = 0 \\ \Rightarrow w_{id}^{\tau-1} \left( \sum_{j=1}^n \tau u_{ij} (\|x_{jd} - v_{id}\|^2 + \Phi(x_{jd} | v_{id}, \Sigma_{id})) + \alpha \tau \right) = \lambda_2 \\ \Rightarrow w_{id} = & \left( \frac{\lambda_2}{\sum_{j=1}^n \tau u_{ij} (\|x_{jd} - v_{id}\|^2 + \Phi(x_{jd} | v_{id}, \Sigma_{id})) + \alpha \tau} \right)^{\frac{1}{\tau-1}} \end{aligned} \quad (23)$$

according to  $\sum_{d=1}^k w_{id} = 1$ , then

$$\begin{aligned} \sum_{d=1}^k w_{id} = & \sum_{d=1}^k \left( \frac{\lambda_2}{\sum_{j=1}^n \tau u_{ij} (\|x_{jd} - v_{id}\|^2 + \Phi(x_{jd} | v_{id}, \Sigma_{id})) + \alpha \tau} \right)^{\frac{1}{\tau-1}} = 1 \\ \Rightarrow \left( \frac{\lambda_2}{\tau} \right)^{\frac{1}{\tau-1}} \sum_{d=1}^k \left( \frac{1}{\sum_{j=1}^n u_{ij} (\|x_{jd} - v_{id}\|^2 + \Phi(x_{jd} | v_{id}, \Sigma_{id})) + \alpha} \right)^{\frac{1}{\tau-1}} = 1 \\ \Rightarrow \left( \frac{\lambda_2}{\tau} \right)^{\frac{1}{\tau-1}} = & \frac{1}{\sum_{d=1}^k \left( \frac{1}{\sum_{j=1}^n u_{ij} (\|x_{jd} - v_{id}\|^2 + \Phi(x_{jd} | v_{id}, \Sigma_{id})) + \alpha} \right)^{\frac{1}{\tau-1}}} \end{aligned} \quad (24)$$

We have

$$\begin{aligned} w_{id} = & \left( \frac{\lambda_2}{\sum_{j=1}^n \tau u_{ij} (\|x_{jd} - v_{id}\|^2 + \Phi(x_{jd} | v_{id}, \Sigma_{id})) + \alpha \tau} \right)^{\frac{1}{\tau-1}} \\ = & \left( \frac{1}{\sum_{j=1}^n u_{ij} (\|x_{jd} - v_{id}\|^2 + \Phi(x_{jd} | v_{id}, \Sigma_{id})) + \alpha} \right)^{\frac{1}{\tau-1}} \\ \cdot & \frac{1}{\sum_{d=1}^k \left( \frac{1}{\sum_{j=1}^n u_{ij} (\|x_{jd} - v_{id}\|^2 + \Phi(x_{jd} | v_{id}, \Sigma_{id})) + \alpha} \right)^{\frac{1}{\tau-1}}} \\ = & \frac{\left( \frac{1}{\sum_{j=1}^n u_{ij} (\|x_{jd} - v_{id}\|^2 + \Phi(x_{jd} | v_{id}, \Sigma_{id})) + \alpha} \right)^{\frac{1}{\tau-1}}}{\sum_{d=1}^k \left( \frac{1}{\sum_{j=1}^n u_{ij} (\|x_{jd} - v_{id}\|^2 + \Phi(x_{jd} | v_{id}, \Sigma_{id})) + \alpha} \right)^{\frac{1}{\tau-1}}} \end{aligned} \quad (25)$$

Finally, based on the iterative computation of the above equations, we obtain the membership matrix  $U$ , the clustering center  $V$ , the covariance matrix  $\Sigma$ , and the fuzzy weights  $W$ . The steps for their detailed calculation are given in **Algorithm 1**.

**Algorithm 1:** Algorithm to solve problem (17)

---

**Data:** image data  $X$ , membership matrix  $U$ , clustering center  $V$ , cluster number  $n$ , minimum error  $\eta = 10^{-5}$ , fuzzy weighting factor  $\tau = 2$ , clustering adjustment factors  $\alpha = 0.1$  and  $\gamma = 0.3$ , maximum number of iterations  $T$ .

- 1 Initialize  $U^{t=0}$ ,  $V^{t=0}$ , and cluster number  $n$ , using Eq. (10), Eq. (11), and Eq. (2);
- 2 **while** not converged **do**
- 3     Update the membership matrix  $U^t$ , using the Eq. (20);
- 4     Update the clustering center  $V^t$ , using Eq. (21);
- 5     Update the covariance  $\Sigma^t$ , using Eq. (22);
- 6     Update the fuzzy weight  $W^t$ , using Eq. (25);
- 7     Compute objective function  $J^t$ , using Eq. (17);
- 8      $t \leftarrow t + 1$ ;
- 9     **if**  $|J_{t+1} - J_t| \leq \eta$  **or**  $t > T$  **then**
- 10         break
- 11     **end**
- 12 **end**
- 13 **return** membership matrix  $U$ .

---

### 3.6. Convergence analysis

In this section, we show that the proposed algorithm is convergent, which means that Eq. (17) can reach the local minimum value. The proof procedure is as follows.

**Theorem 1.** Fixing the clustering center  $v_{id}$ , the fuzzy weight  $w_{id}$ , and the covariance matrix  $\Sigma_{id}$ , then the membership matrix  $u_{ij}$  in Eq. (20) is the local minimum of Eq. (17).

**Proof.** If  $u_{ij}$  is demonstrated to be a local minimum of Eq. (17), it is necessary to show that it is concave at the extremum point. Since  $u_{ij}$  in Eq. (20) is its extremum point at this time, we only need to prove that the second-order partial derivative in Eq. (17) is positive. The second-order partial derivative of Eq. (17) concerning  $u_{ij}$  is as follows:

$$\begin{aligned} \frac{\partial^2 J}{\partial u_{ij}^2} &= \frac{\partial \left( \sum_{d=1}^k w_{id}^\tau (\|x_{jd} - v_{id}\|^2 + \Phi(x_{jd} | v_{id}, \Sigma_{id})) + \gamma(\ln u_{ij} + 1) - \lambda_1 \right)}{\partial u_{ij}} \\ &\Rightarrow \frac{\partial^2 J}{\partial u_{ij}^2} = \frac{\gamma}{u_{ij}} \end{aligned} \quad (26)$$

Since  $u_{ij} > 0$  and when  $\gamma > 0$ , then  $\frac{\partial^2 J}{\partial u_{ij}^2} > 0$ , it is known that the above Eq. (26) is positive. Therefore,  $u_{ij}$  in Eq. (20) is the local minimum of Eq. (17).

**Theorem 2.** Fixing the membership matrix  $u_{ij}$ , the fuzzy weight  $w_{id}$  and the covariance matrix  $\Sigma_{id}$ , then the clustering center  $v_{id}$  in Eq. (21) is the local minimum of Eq. (17).

**Proof.** The process of proving **Theorem 2** is the same as that of **Theorem 1**. We only need to show that the second-order partial derivative of  $v_{id}$  in Eq. (17) is positive. Its second-order partial derivative with respect to  $v_{id}$  is as follows.

$$\begin{aligned} \frac{\partial^2 J}{\partial v_{id}^2} &= \frac{\sum_{j=1}^n u_{ij} w_{id}^\tau ((x_{jd} - v_{id}) + \Sigma_{id}^{-1}(x_{jd} - v_{id}))}{\partial v_{id}} \\ &\Rightarrow \frac{\partial^2 J}{\partial v_{id}^2} = \sum_{j=1}^n u_{ij} w_{id}^\tau (1 + \Sigma_{id}^{-1}) \end{aligned} \quad (27)$$

In the above equation, since  $\Sigma_{id} = E[(x_{jd} - v_{id})(x_{jd} - v_{id})]$ , it is semi-positive definite, and the value of its determinant is non-negative, the above equation is positive. Therefore,  $v_{id}$  in Eq. (21) is also the local minimum of Eq. (17).

**Theorem 3.** Fixing the membership matrix  $u_{ij}$ , the clustering center  $v_{id}$ , and the covariance matrix  $\Sigma_{id}$ , then the fuzzy weight  $w_{id}$  in Eq. (25) is the local minimum of Eq. (17).

**Proof.** In the same way, we only need to demonstrate that the second-order partial derivative of Eq. (17) with respect to  $w_{id}$  is positive, and its second-order partial derivative is

$$\begin{aligned} \frac{\partial^2 J}{\partial w_{id}^2} &= \frac{\partial \left( \sum_{j=1}^n \tau u_{ij} w_{id}^{\tau-1} (\|x_{jd} - v_{id}\|^2 + \Phi(x_{jd} | v_{id}, \Sigma_{id})) + \alpha \tau w_{id}^{\tau-1} - \lambda_2 \right)}{\partial w_{id}} \\ &\Rightarrow \frac{\partial^2 J}{\partial w_{id}^2} \\ &= \tau(\tau - 1) \left( \sum_{j=1}^n u_{ij} w_{id}^{\tau-2} (\|x_{jd} - v_{id}\|^2 + \Phi(x_{jd} | v_{id}, \Sigma_{id})) + \alpha w_{id}^{\tau-2} \right) \end{aligned} \quad (28)$$

It can be found that when  $\tau > 1$  and  $\alpha > 0$ , the above equation is positive, which proves that  $w_{id}$  in Eq. (25) is the local minimum of Eq. (17).

From the proofs of the above three **Theorems**, we can conclude that the proposed algorithm in this paper is convergent.

## 4. Experiments

To demonstrate the effectiveness of our proposed algorithm, we verified it from four aspects: 1. The effect of the initialization settings on the proposed algorithm; 2. Verify the validity of our distance metric; 3. Validity of fuzzy weight; and 4. The feasibility and validity of our algorithm on different images of the Berkeley Segmentation Dataset (BSDS500) (Arbelaez et al., 2010) and Stanford Background Dataset (SBD) (Gould et al., 2009). We conduct a series of qualitative and quantitative experimental comparisons on the database BSDS500. The comparison algorithms present are based on fuzzy theory, such as FCM, FCM\_S1, FCM\_S2, FGFCM, KWFLICM, FRFCM, DSFCM, FCM\_SICM, SFFCM, RSSFCA, AFCF, CGFFCM and FSC\_LNML. These are used to solve image segmentation problems. All experiments are performed on a PC workstation with a 3.6 GHz CPU and 8 GB RAM using MATLAB 2019a.

### 4.1. Parameter settings

In our experiments, the weighting exponent, the minimum error threshold, and the maximum number of iterations are the indispensable parameters of these comparison algorithms, which are set to 2,  $10^{-4}$ , and 100, respectively. Furthermore, other parameters are set following their original papers. Some comparison algorithms require a filtering window whose size is set to  $3 \times 3$ . In FCM, FCM\_S1, and FCM\_S2,  $\alpha$  is the control parameter related to local denoising and is generally set to  $\alpha = 3.8$ . For FGFCM, the spatial scale and the gray-level scale factors are  $\lambda_s = 3$  and  $\lambda_g = 5$ . In addition, KWFLICM and DSFCM are required to set the weighting exponent, the minimum error threshold, the maximum number of iterations, and the cluster number. In FRFCM, the structuring element and the filter window sizes are set to  $3 \times 3$ . The RSSFCA requires a regularization parameter  $\gamma = 0.2$ . For SFFCM and AFCF, their superpixel algorithm MMGR-WT has two parameters:  $r_1 = 2$  and  $\eta = 10^{-4}$ . Among them, the parameters in FSC\_LNML are set as follows, the local window size  $l = 7$ , the nonlocal window radius  $S = 15$ , the decay parameter of the exponential function  $g = 25$ , the weight regularity parameter  $\gamma = 0.7$ , the fuzzy index  $\tau = 2$ , and the variance control parameter  $\sigma = 500$ . The parameter settings in our improved superpixel algorithm are the same as those in the MMGR-WT algorithm. Moreover, The parameters of the initialization algorithm are set to  $\lambda_1 = 5$ ,  $\lambda_2 = 2$ , and  $\delta = 0.8$ . The main parameters in our objective function are the clustering adjustment coefficients, which are set to  $\alpha = 0.1$  and  $\gamma = 0.3$ , respectively.

### 4.2. Evaluation metrics

In this paper, we utilize four commonly employed evaluation metrics (Lei et al., 2019): probabilistic random index (PRI), variation of information (VoI),



**Fig. 4.** Comparison of the image segmentation results obtained by the proposed algorithm using four initialization methods. (a) Inputs, (b) The results obtained by our initialization method, (c) The results of manually setting the number of clusters ( $n = 3$ ) and randomly initializing the membership matrix, (d) The results of manually setting the number of clusters ( $n = 3$ ) and initializing the membership matrix using FCM, (e) The results of using the AFCF algorithm to obtain the number of clusters and initialize the membership matrix.

global consistency error (GCE), and boundary displacement error (BDE). These metrics are employed to assess the segmentation results achieved by both the proposed algorithm and the comparison algorithm. Their utility lies in their ability to evaluate segmentation performance from diverse perspectives, ensuring a comprehensive and accurate evaluation. Among them, PRI is the ratio of the number of pixels overlapping the segmentation result and the ground truth to the total number of pixels. VoI defines the distance between the segmentation result and the ground truth as the average conditional entropy. Moreover, it measures the degree of randomness in the segmentation result that cannot be covered by the ground truth. GCE measures the degree of agreement between the image segmentation result and the ground truth. BDE computes the average displacement error between the image segmentation result and the boundary pixels in the ground truth. The larger the PRI value and the smaller the VoI, GCE, and BDE values in the quantitative results, the closer the segmentation result is to the ground truth, indicating the superior performance of the proposed algorithm.

#### 4.3. The effect of the initialization settings on the proposed algorithm

To demonstrate the effectiveness of the proposed adaptive initialization algorithm, we conducted experiments by comparing the following three types of initialization settings: (1) Manually setting the number of clusters and randomly initializing the membership matrix; (2) Manually setting the number of clusters and initializing the membership matrix using FCM; (3) Using AFCF to obtain the initialization of the cluster number and the membership matrix.

**Table 1**

Comparison of the average objective evaluation metrics for the results in Fig. 4. The b, c, d, and e in Table 1 correspond to those in Fig. 4.

	b	c	d	e
PRI	0.8114	0.6610	0.6902	0.6889
VoI	1.4355	1.7896	1.6290	1.6083
GCE	0.0468	0.1324	0.1894	0.0937
BDE	9.4649	14.5987	11.0387	9.9113

**Table 2**

The number of clusters automatically obtained by the two initialization algorithms.

	3063	12 003	113 044	239 007	134 008	8068
OURS	3	2	2	3	2	5
AFCF	4	2	3	3	2	2

**Table 3**

Performance of the four evaluation metrics for different distances in Fig. 5.

	Our distance	Euclidean distance	Non-Euclidean distance
PRI	0.7452	0.6380	0.6832
VoI	1.7353	2.1648	2.1195
GCE	0.0899	0.1762	0.1734
BDE	10.7465	17.8407	11.6191

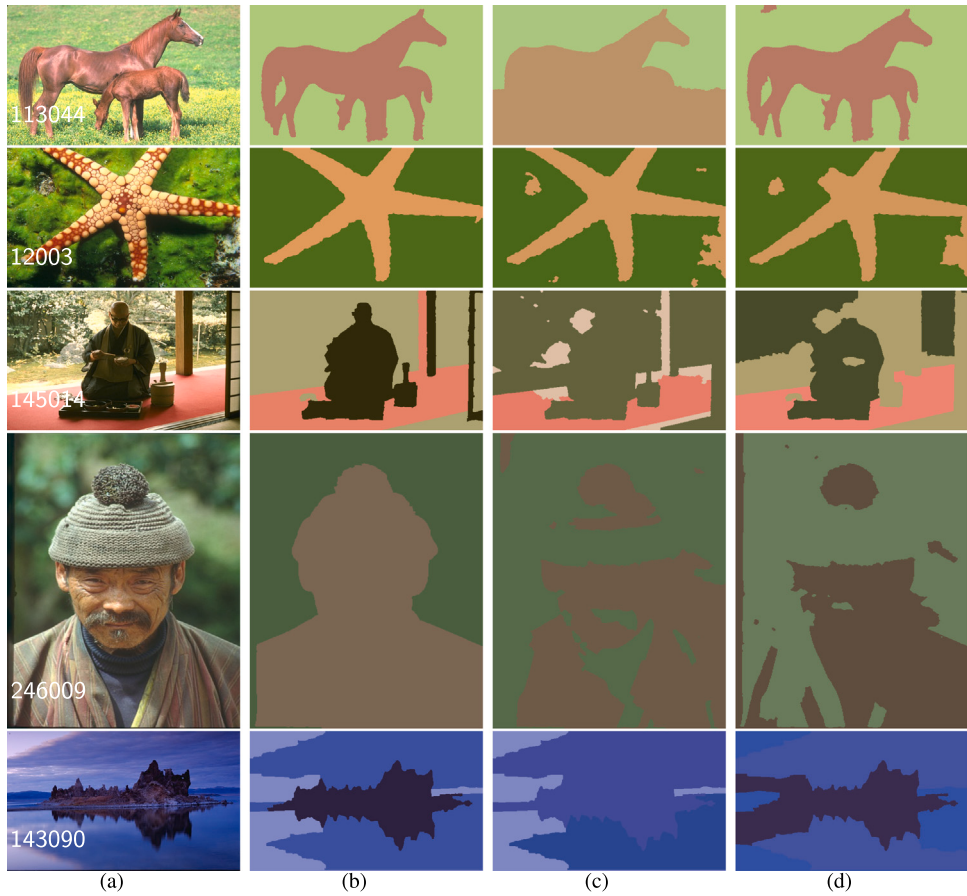


**Fig. 5.** Comparison of the results of different distance metrics. (a) Inputs, (b) Our distance, (c) Euclidean distance, (d) Non-Euclidean distance.

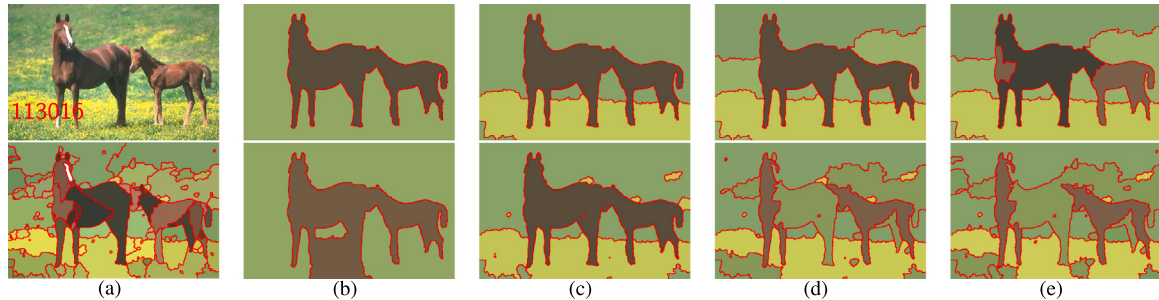


**Fig. 6.** Comparison of segmentation results with and without fuzzy weights under the different number of clusters. The upper layer is the segmentation result with fuzzy weights, and the lower layer is the segmentation result without fuzzy weights. From left to right, the segmentation results are (a). original image and superpixel image, (b). segmentation results at  $n = 2$ , (c). segmentation results at  $n = 3$ , (d). segmentation results at  $n = 4$ , (e). segmentation results at  $n = 5$ .

**Table 4**

Performance of fuzzy weights for the four objective evaluation metrics in the database BSDS500.

	With fuzzy weights	Without fuzzy weights
PRI	0.7514	0.7236
Vol	2.2045	2.3518
GCE	0.2889	0.2832
BDE	12.9125	13.9674

**Fig. 4** and **Table 1** compare the image segmentation results obtained by the proposed algorithm using four initialization methods. It is evident that our initialization method yields the most favorable segmentation results. Additionally, varying outcomes with different initialization methods suggest that the structure of our proposed algorithm does not inherently ensure

convergence to the optimal solution. However, through proper initialization, we can achieve convergence towards this optimal solution. The comparison of the four objective evaluation metric values in **Table 1** corresponds to **Fig. 4**, which demonstrates the effectiveness of our proposed initialization setting method.

In addition, in **Fig. 4**, the number of clusters to be set manually is  $n = 3$ . **Table 2** shows the cluster number obtained automatically by our proposed initialization algorithm and AFCF. According to image content, we can conclude that the number of clusters is more reasonable obtained by our initialization algorithm based on SSC. Moreover, Among the four initialization methods, fixed cluster numbers and random or simplistic initializations yield less satisfactory results. However, the initialization of cluster numbers obtained by the designed algorithm according to the features of the images is more reasonable. As shown in **Table 1**, our proposed initialization algorithm and the AFCF initialization algorithm outperform the other two approaches, which

shows that the designed algorithm based on the image features can improve the clustering effect. Moreover, it is also demonstrated that the initialization approach obtains the cluster number and the membership matrix, correlating them to enhance the proposed algorithm's convergence towards the optimal solution.

#### 4.4. Verify the validity of our distance metric

The choice of distance metric plays a crucial role as it acts as a determining factor for clustering attribution. In our study, we introduce a novel distance metric that amalgamates Euclidean and non-Euclidean distances. This approach capitalizes on the strengths of the Euclidean distance in clustering low-dimensional data while also effectively characterizing similarity in high-dimensional feature spaces. Consequently, this metric empowers our proposed algorithm to achieve high clustering accuracy.

To validate the effectiveness of our proposed distance metric, which combines Euclidean and non-Euclidean distances, we conducted comparisons by replacing the new distance metric separately with Euclidean and non-Euclidean distances within our method.

**Fig. 5** displays the image segmentation results obtained by our algorithm utilizing different distance metrics. Our proposed distance metric demonstrates an exceptional ability to cluster diverse features into a single class, particularly evident in the image labeled "246009". In contrast, the other two distances struggle to achieve this level of performance.

**Table 3** showcases the mean values of the four objective evaluation metrics corresponding to the different distances depicted in **Fig. 5**. Across all metrics, our proposed approach outperforms the other two distances significantly. Hence, based on the insights gleaned from **Fig. 5** and **Table 3**, we confidently assert the effectiveness of our proposed distance metric, which combines Euclidean and non-Euclidean distances, in clustering.

#### 4.5. Validity of fuzzy weights

In this subsection, we verify the validity of fuzzy weights for the proposed algorithm. Previously, many works have confirmed the existence of different importance (weight) of individual features to the clustering centers. However, we still need to verify the validity of the fuzzy weights in our proposed algorithm.

As shown in **Fig. 6**, the segmentation results are compared with and without fuzzy weights under the different number of clusters. When our proposed algorithm lacks fuzzy weights, the segmentation results depict unsatisfactory clustering scenarios, including isolated feature regions and misaligned clusters. Conversely, with the inclusion of fuzzy weights in our proposed algorithm, the segmentation results exhibit accurate clustering of distinguishable superpixel features, even across different cluster numbers. Moreover, as shown in **Table 4**, the performance of our proposed algorithm with fuzzy weights is slightly worse than that of the proposed algorithm without fuzzy weights in terms of GCE, while the former significantly outperforms the latter in terms of PRI, VoI, and BDE. Therefore, this substantiates the effectiveness of fuzzy weights in enhancing the accuracy of image clustering. Furthermore, we can conclude that the incorporation of fuzzy weights enables the assignment of appropriate weights to each superpixel feature, thereby controlling feature correlations, reducing interference from irrelevant or redundant superpixel features, and supplementing the limitations of distance metrics.

#### 4.6. Result on color image

To demonstrate the effectiveness and superiority of the proposed algorithm for image segmentation, we conducted tests and validations on the BSDS500 and SBD datasets. Additionally, the parameters utilized by the comparison algorithms adhere to the settings specified in their respective papers. For the FCM-based algorithm, where clustering parameters require manual adjustment, the number of clusters is set to 3 to ensure a fair comparison.

**Figs. 7** and **8** display segmentation results obtained from both our proposed algorithm and the comparison algorithm for simple and complex scenes. An observation reveals that subjective segmentation outcomes of FCM-based

**Table 5**

Performance comparison of different algorithms on the BSDS500 dataset. The best values are highlighted.

	PRI	VoI	GCE	BDE
FCM	0.69	2.93	0.38	14.47
FCM_S1	0.70	2.87	0.37	14.30
FCM_S2	0.69	2.86	0.36	14.42
FGFCM	0.69	2.85	0.36	14.24
KWFLICM	0.72	2.80	0.35	14.27
FRFCM	0.73	2.60	0.30	13.98
DSFCM	0.70	2.82	0.36	14.63
SFFCM	0.72	2.31	0.26	14.35
RSSFCA	0.73	2.28	0.28	14.46
FCM_SICM	0.67	2.87	0.34	14.78
AFCF	0.74	2.22	<b>0.22</b>	13.93
CGFFCM	0.73	2.35	0.32	14.33
FSC_LNML	0.69	2.25	0.24	14.52
OURS	<b>0.75</b>	<b>2.20</b>	0.29	<b>12.91</b>

**Table 6**

Performance comparison of different algorithms on the SBD dataset. The best values are highlighted.

	PRI	VoI	GCE	BDE
FCM	0.66	2.31	0.32	10.52
FCM_S1	0.67	2.26	0.31	10.44
FCM_S2	0.68	2.25	0.30	10.50
FGFCM	0.67	2.25	0.31	10.39
KWFLICM	0.68	2.19	0.29	10.23
FRFCM	0.71	2.05	0.28	9.90
DSFCM	0.69	2.23	0.30	10.63
SFFCM	0.65	<b>1.75</b>	0.19	11.05
RSSFCA	0.66	1.78	0.20	11.26
FCM_SICM	0.62	2.07	0.25	11.59
AFCF	0.74	1.95	<b>0.18</b>	10.13
CGFFCM	0.73	2.10	0.24	11.03
FSC_LNML	0.69	2.25	0.22	10.63
OURS	<b>0.76</b>	1.81	0.20	<b>9.79</b>

algorithms, not leveraging superpixel technology, tend to be unsatisfactory. These approaches lack the constraints of local information, struggling to cluster target regions effectively within the images. In contrast, algorithms based on the superpixel technique aptly capture and express target information, significantly enhancing visual effects. This analysis underscores the effectiveness of superpixel techniques in substantially improving the segmentation outcomes of FCM-based algorithms.

In **Tables 5** and **6**, FCM, FCM\_S1, and FCM\_S2 exhibit similar performance in PRI, VoI, GCE, and BDE, largely due to their comparable algorithm structures. Although FGFCM enhances computational speed relative to the FCM\_S algorithm, it does not notably improve image segmentation accuracy. KWFLICM elevates segmentation performance compared to previous methodologies by introducing a kernel distance metric and leveraging local information. DSFCM stands out for its noise immunity owing to a regularization term within the FCM structure. However, its segmentation results are somewhat unsatisfactory. **Fig. 7**, **Fig. 8**, and **Table 5** collectively demonstrate the significant enhancement in image segmentation achieved by employing superpixel algorithms like FRFCM, SFFCM, RSSFCA, and AFCF. Notably, these methods exhibit substantial improvements in PRI, VoI, and BDE metrics. Additionally, both CGFFCM and FSC\_LNML employ feature weights to refine clustering accuracy. While CGFFCM places more emphasis on feature weights, FSC\_LNML prioritizes local variance and non-local information.

Compared to the comparison algorithms, our proposed algorithm performs better, as shown in **Figs. 7** and **8**. In **Table 5**, our proposed algorithm demonstrates superior performance in terms of PRI, VoI, and BDE on the BSDS500 dataset. Meanwhile, in **Table 6**, our proposed algorithm excels in PRI and BDE on the SBD dataset. Notably, the BDE metric showcases a significant improvement of nearly 7.7%, underscoring the algorithm's exceptional edge characteristics for image segmentation. Furthermore, our proposed algorithm



**Fig. 7.** Visual comparison of segmentation results on relatively simple scene images using fourteen algorithms.

exhibits competitive performance across other evaluation metrics. This comprehensive analysis and comparison unequivocally validate the effectiveness and robustness of the proposed algorithm in this paper.

#### 4.7. Analysis of computational complexity

The computational complexity of an algorithm is a crucial metric for evaluating its performance. In Table 7,  $N$  denotes the number of image pixels,

$c$  represents the number of clusters,  $t$  signifies the number of iterations, and  $t'$  denotes the iterations of SSC. Additionally,  $\omega$  signifies the filter window size, and  $q$  represents the grayscale value of the image. Notably,  $N'$  refers to the significantly fewer number of superpixels compared to  $N$ ,  $T'$  indicates fewer iterations than  $t$ , and  $O(M(c))$  symbolizes the computational complexity of Newton's method.

The computational load of our proposed algorithm comprises three primary components: the superpixel algorithm, the SSC-based initialization algorithm,



**Fig. 8.** Visual comparison of segmentation results on relatively complex scene images using fourteen algorithms.

and the proposed objective function. The superpixel algorithm, based on the MMGR-WT algorithm, has a computational complexity of  $O(N \times T')$ . The SSC-based initialization algorithm has a complexity of  $O(N'^2 \times t')$ , while the solution complexity of our proposed objective function is  $O(N' \times c \times m \times t)$ . Consequently, the total computational complexity of our proposed algorithm is  $O(N \times T' + N'^2 \times t' + N' \times c \times m \times t)$ . In Table 7, our proposed algorithm, when formally compared to FCM, FCM\_S1, FCM\_S2, FGFCM, FRFCM, SFFCM,

RSSFCA, FCM\_SICM, and AFCF, exhibits a complex structure and higher computational complexity. However, it is lower than KWFLICM, DSFCM, CGFFCM, and FSC\_LNML. Additionally, the computational complexity of our proposed algorithm is contingent upon the number of superpixels. Clearly, our proposed algorithm does not offer the highest computational efficiency. Nevertheless, it stands as an adaptive and robust image segmentation algorithm.

**Table 7**  
Computational complexity of different algorithms.

Methods	Computational complexity
FCM	$O(N \times c \times t)$
FCM_S1	$O(N \times \omega^2 + N \times c \times t)$
FCM_S2	$O(N \times \omega^2 + N \times c \times t)$
FGFCM	$O(N \times \omega^2 + q \times c \times t)$
KWFICM	$O(N \times (\omega + 1)^2 + N \times \omega^2 \times c \times t)$
FRFCM	$O(N \times \omega^2 + q \times c \times t)$
DSFCM	$O(N \times \omega^2 \times c \times t)$
SFFCM	$O(N \times T' + N' \times c \times t)$
RSSFCA	$O(N \times (M(C) + c) \times t + N \times c \times t)$
FCM_SICM	$O(N \times q \times \log(N \times q) + 2N \times \omega^2 + N \times c \times t)$
AFCF	$O(N \times T' + N' \times c \times t \times 2)$
CGFFCM	$O(4N \times c \times m \times t)$
FSC_LNML	$O(N \times \omega^2 + N \times c \times m \times t)$
OURS	$O(N \times T' + N'^2 \times t' + N' \times c \times m \times t)$

## 5. Conclusion

In this paper, we propose an adaptive fuzzy weighted C-mean image segmentation algorithm that addresses two fundamental issues encountered in FCM-based algorithms: initialization settings and distance metrics. The former concern can often lead to segmentation results getting trapped in local minima, while the latter may fail to adequately capture variability among high-dimensional features, resulting in unsatisfactory image segmentation. We utilize an enhanced SSC algorithm based on the superpixel image for initialization settings, deriving the initial number of clusters and the membership matrix. Comparative analysis against various commonly used initialization methods confirms that our approach ensures optimal convergence of the algorithm. Additionally, our proposed distance metric, combining Euclidean and non-Euclidean distances, along with the integration of fuzzy weights, effectively mitigates redundant feature interference, resulting in more reasonable clustering outcomes. The comparison across the BSDS500 and SBD datasets with several other advanced algorithms has demonstrated the effectiveness and robustness of our proposed algorithm.

However, an excess of control factors can lead to a bloated algorithm structure. This increase in complexity results in longer computing times, prompting the need to optimize the proposed algorithm for improved computational efficiency without compromising accuracy. Our next step involves exploring effective feature combinations and investigating relatively simple and robust fuzzy structures.

## CRediT authorship contribution statement

**Sensen Song:** Conceptualization, Methodology, Software. **Zhenhong Jia:** Data curation, Supervision, Writing – original draft. **Fei Shi:** Writing – review & editing. **Junnan Wang:** Writing – review & editing. **Dongdong Ni:** Writing – review & editing.

## Declaration of competing interest

We confirm that there are no known conflicts of interest associated with this publication, and there has been no significant financial support for this work that could have influenced its outcome.

We confirm that the manuscript has been read and approved by all named authors and that there are no other persons who satisfied the criteria for authorship but are not listed. We further confirm that we have approved the order of authors listed in the manuscript.

We confirm that we have given due consideration to the protection of intellectual property associated with this work and that there are no impediments to publication, including the timing of publication, for intellectual property. In so doing, we confirm that we have followed the regulations of our institutions concerning intellectual property.

We understand that the Corresponding Author is the sole contact for the Editorial process (including Editorial Manager and direct communications with the office). He is responsible for communicating with the other authors about progress, submissions of revisions, and final approval of proofs.

The authors do not have financial and personal relationships with other people or organizations that could inappropriately influence (bias) their work.

## Data availability

The datasets generated and analyzed during this study are available in the Berkeley Segmentation Dataset and Benchmark repository: <https://www2.eecs.berkeley.edu/Research/Projects/CS/vision/grouping/resources.html> and the Standford Background Dataset repository: <https://dags.stanford.edu/projects/scenedataset.html>.

## Acknowledgments

This work was supported by the National Natural Science Foundation of China (No. U1803261 and 62261053), the Natural Science Foundation of Xin-Jiang under Grant 2022D01C58, and Scientific Research Plan of Universities in Xinjiang Uygur Autonomous Region under Grant XJEDU2019Y006.

## References

- Achanta, R., Shaji, A., Smith, K., Lucchi, A., Fua, P., Süstrunk, S., 2012. SLIC superpixels compared to state-of-the-art superpixel methods. *IEEE Trans. Pattern Anal. Mach. Intell.* 34 (11), 2274–2282.
- Ahmed, M.N., Yamany, S.M., Mohamed, N., Farag, A.A., Moriarty, T., 2002. A modified fuzzy c-means algorithm for bias field estimation and segmentation of MRI data. *IEEE Trans. Med. Imaging* 21 (3), 193–199.
- Amane, M., Aissaoui, K., Berrada, M., 2023. Enhancing learning object analysis through fuzzy C-means clustering and web mining methods. *Emerg. Sci. J.* 7 (3), 799–807.
- Arbelaez, P., Maire, M., Fowlkes, C., Malik, J., 2010. Contour detection and hierarchical image segmentation. *IEEE Trans. Pattern Anal. Mach. Intell.* 33 (5), 898–916.
- Bajgiran, A.H., Mardikoraeem, M., Soofi, E.S., 2021. Maximum entropy distributions with quantile information. *European J. Oper. Res.* 290 (1), 196–209.
- Ban, Z., Liu, J., Cao, L., 2018. Superpixel segmentation using Gaussian mixture model. *IEEE Trans. Image Process.* 27 (8), 4105–4117.
- Bezdek, J.C., 2013. *Pattern Recognition with Fuzzy Objective Function Algorithms*. Springer Science & Business Media.
- Bezdek, J.C., Ehrlich, R., Full, W., 1984. FCM: The fuzzy c-means clustering algorithm. *Comput. Geosci.* 10 (2–3), 191–203.
- Bhadane, P., Menon, R., Jain, R., Joshi, D., Ravikar, A.A., 2022. Integrated framework for inclusive town planning using fuzzy analytic hierarchy method for a semi urban town. *Civ. Eng. J.* 8 (12), 2768–2778.
- Boyd, S., Parikh, N., Chu, E., Peleato, B., Eckstein, J., 2010. Distributed optimization and statistical learning via the alternating direction method of multipliers. *Mach. Learn.* 3 (1), 1–122.
- Cai, W., Chen, S., Zhang, D., 2007. Fast and robust fuzzy c-means clustering algorithms incorporating local information for image segmentation. *Pattern Recognit.* 40 (3), 825–838.
- Chen, S., Zhang, D., 2004. Robust image segmentation using FCM with spatial constraints based on new kernel-induced distance measure. *IEEE Trans. Syst. Man Cybern. B* 34 (4), 1907–1916.
- Dollár, P., Zitnick, C.L., 2014. Fast edge detection using structured forests. *IEEE Trans. Pattern Anal. Mach. Intell.* 37 (8), 1558–1570.
- Dunn, J., 1973. A fuzzy relative of the ISODATA process and its use in detecting compact well-separated clusters. *J. Cybern.* 3 (3), 32–57.
- Elhamifar, E., Vidal, R., 2013. Sparse subspace clustering: Algorithm, theory, and applications. *IEEE Trans. Pattern Anal. Mach. Intell.* 35 (11), 2765–2781.

- Emami, H., Derakhshan, F., 2015. Integrating fuzzy K-means, particle swarm optimization, and imperialist competitive algorithm for data clustering. *Arab. J. Sci. Eng.* 40 (12), 3545–3554.
- Eskenazis, A., Nayar, P., Tkocz, T., 2018. Gaussian mixtures: entropy and geometric inequalities. *Ann. Probab.* 46 (5), 2908–2945.
- Friedman, K., Shimony, A., 1971. Jayne's maximum entropy prescription and probability theory. *J. Stat. Phys.* 3 (4), 381–384.
- Gan, G., Wu, J., Yang, Z., 2006. A fuzzy subspace algorithm for clustering high dimensional data. In: International Conference on Advanced Data Mining and Applications. Springer, pp. 271–278.
- Gong, M., Liang, Y., Shi, J., Ma, W., Ma, J., 2012. Fuzzy c-means clustering with local information and kernel metric for image segmentation. *IEEE Trans. Image Process.* 22 (2), 573–584.
- Gou, X., Xu, Z., Liao, H., 2017. Hesitant fuzzy linguistic entropy and cross-entropy measures and alternative queuing method for multiple criteria decision making. *Inform. Sci.* 388, 225–246.
- Gould, S., Fulton, R., Koller, D., 2009. Decomposing a scene into geometric and semantically consistent regions. In: 2009 IEEE 12th International Conference on Computer Vision. IEEE, pp. 1–8.
- Guo, Y., Wang, R., Zhou, J., Chen, Y., Jiang, H., Han, S., Wang, L., Du, T., Ji, K., Zhao, Y.-o., et al., 2022. Soft subspace fuzzy clustering with dimension affinity constraint. *Int. J. Fuzzy Syst.* 1–19.
- Havens, T.C., Bezdek, J.C., Leckie, C., Hall, L.O., Palaniwami, M., 2012. Fuzzy c-means algorithms for very large data. *IEEE Trans. Fuzzy Syst.* 20 (6), 1130–1146.
- Hu, H., Lin, Z., Feng, J., Zhou, J., 2014. Smooth representation clustering. In: Proceedings of the IEEE Conference on Computer Vision and Pattern Recognition. pp. 3834–3841.
- Jia, X., Lei, T., Du, X., Liu, S., Meng, H., Nandi, A.K., 2020. Robust self-sparse fuzzy clustering for image segmentation. *IEEE Access* 8, 146182–146195.
- Karayannis, N.B., 1994. MECA: Maximum entropy clustering algorithm. In: Proceedings of 1994 IEEE 3rd International Fuzzy Systems Conference. IEEE, pp. 630–635.
- Krinidis, S., Chatzis, V., 2010. A robust fuzzy local information C-means clustering algorithm. *IEEE Trans. Image Process.* 19 (5), 1328–1337.
- Lei, T., Jia, X., Zhang, Y., He, L., Meng, H., Nandi, A.K., 2018a. Significantly fast and robust fuzzy c-means clustering algorithm based on morphological reconstruction and membership filtering. *IEEE Trans. Fuzzy Syst.* 26 (5), 3027–3041.
- Lei, T., Jia, X., Zhang, Y., Liu, S., Meng, H., Nandi, A.K., 2018b. Superpixel-based fast fuzzy C-means clustering for color image segmentation. *IEEE Trans. Fuzzy Syst.* 27 (9), 1753–1766.
- Lei, T., Liu, P., Jia, X., Zhang, X., Meng, H., Nandi, A.K., 2019. Automatic fuzzy clustering framework for image segmentation. *IEEE Trans. Fuzzy Syst.* 28 (9), 2078–2092.
- Li, Z., Chen, J., 2015. Superpixel segmentation using linear spectral clustering. In: Proceedings of the IEEE Conference on Computer Vision and Pattern Recognition. pp. 1356–1363.
- Li, C.-G., You, C., Vidal, R., 2017. Structured sparse subspace clustering: A joint affinity learning and subspace clustering framework. *IEEE Trans. Image Process.* 26 (6), 2988–3001.
- Nayak, J., Naik, B., Behera, H., 2015. Fuzzy C-means (FCM) clustering algorithm: a decade review from 2000 to 2014. *Comput. Intell. Data Min.* 2, 133–149.
- Nie, S.-D., Li-Hong, L., Chen, Z.-X., 2007. A CI feature-based pulmonary nodule segmentation using three-domain mean shift clustering. In: 2007 International Conference on Wavelet Analysis and Pattern Recognition, Vol. 1. IEEE, pp. 223–227.
- Osokouei, A.G., Hashemzadeh, M., Asheghi, B., Balafar, M.A., 2021. CGFFCM: cluster-weight and group-local feature-weight learning in fuzzy C-means clustering algorithm for color image segmentation. *Appl. Soft Comput.* 113, 108005.
- Shen, J., Hao, X., Liang, Z., Liu, Y., Wang, W., Shao, L., 2016. Real-time superpixel segmentation by DBSCAN clustering algorithm. *IEEE Trans. Image Process.* 25 (12), 5933–5942.
- Spruyt, V., 2014. The curse of dimensionality in classification. *Comput. Vis. Dummies* 21 (3), 35–40.
- Sun, H., Wang, S., Jiang, Q., 2004. FCM-based model selection algorithms for determining the number of clusters. *Pattern Recognit.* 37 (10), 2027–2037.
- Surono, S., Hsm, Z.A.R., Dewi, D.A., Haryati, A.E., Wijaya, T.T., 2023. Implementation of takagi sugeno kang fuzzy with rough set theory and mini-batch gradient descent uniform regularization. *Emerg. Sci. J.* 7 (3), 791–798.
- Szilagyi, L., Benyo, Z., Szilagyi, S.M., Adam, H., 2003. MR brain image segmentation using an enhanced fuzzy c-means algorithm. In: Proceedings of the 25th Annual International Conference of the IEEE Engineering in Medicine and Biology Society (IEEE Cat. No. 03CH37439), Vol. 1. IEEE, pp. 724–726.
- Wang, Q., Wang, X., Fang, C., Yang, W., 2020. Robust fuzzy c-means clustering algorithm with adaptive spatial & intensity constraint and membership linking for noise image segmentation. *Appl. Soft Comput.* 92, 106318.
- Wang, X., Wang, Y., Wang, L., 2004. Improving fuzzy c-means clustering based on feature-weight learning. *Pattern Recognit. Lett.* 25 (10), 1123–1132.
- Wei, T., Wang, X., Li, X., Zhu, S., 2022. Fuzzy subspace clustering noisy image segmentation algorithm with adaptive local variance & non-local information and mean membership linking. *Eng. Appl. Artif. Intell.* 110, 104672.
- Yang, M.-S., Nataliani, Y., 2017. A feature-reduction fuzzy clustering algorithm based on feature-weighted entropy. *IEEE Trans. Fuzzy Syst.* 26 (2), 817–835.
- Yeung, D.S., Wang, X., 2002. Improving performance of similarity-based clustering by feature weight learning. *IEEE Trans. Pattern Anal. Mach. Intell.* 24 (4), 556–561.
- Zhang, Y., Bai, X., Fan, R., Wang, Z., 2018. Deviation-sparse fuzzy c-means with neighbor information constraint. *IEEE Trans. Fuzzy Syst.* 27 (1), 185–199.
- Zhang, M., Jiang, W., Zhou, X., Xue, Y., Chen, S., 2019. A hybrid biogeography-based optimization and fuzzy C-means algorithm for image segmentation. *Soft Comput.* 23 (6), 2033–2046.
- Zhang, Y., Sun, Z., He, R., Tan, T., 2013. Robust subspace clustering via half-quadratic minimization. In: Proceedings of the IEEE International Conference on Computer Vision. pp. 3096–3103.
- Zhou, J., Chen, L., Chen, C.P., Zhang, Y., Li, H.-X., 2016. Fuzzy clustering with the entropy of attribute weights. *Neurocomputing* 198, 125–134.

**Sensen Song** received the B.S. degrees from Xinjiang Normal University, Urumqi, China, in 2014, and the M.S. and Ph.D. degrees from the School of Information Science and Engineering, Xinjiang University, Urumqi, China. At present, he has been introduced to the Xinjiang University as an A-level Young Talent to engage in teaching and scientific research. His research interests are in the area of image processing.

**Zhenhong Jia** received the B.S. degree from Beijing Normal University, Beijing, China, in 1985, and the M.S. and Ph.D. degrees from Shanghai Jiao Tong University, Shanghai, China, in 1987 and 1995, respectively. He is currently a Professor with the Autonomous University Key Laboratory of Signal and Information Processing Laboratory, Xinjiang University, China. His research interests include digital image processing, optical information detection, and machine learning.

**Fei Shi** received the B.S. and M.S. degrees from the School of Information Science and Engineering, Xinjiang University, Urumqi, China, in 2008 and 2012. He is currently pursuing the Ph.D. degree from the School of Information Science and Engineering, Xinjiang University, China. His research interests include the clarity of video and images under sandstorm weather conditions.

**Junnan Wang** received the B.S. degree in Nanyang Normal University, Henan, China, in 2014. And the M.S. degree Xinjiang University, Xinjiang, China, in 2018. Currently, He is pursuing the Ph.D. degree in Computer Application Technology with Xinjiang University. His research interests include image processing, computer vision.

**Dongdong Ni** received the B.S. and M.S. degrees from the School of Information Science and Engineering, Xinjiang University, Urumqi, China, in 2011 and 2015. He is currently pursuing the Ph.D. degree from the School of Information Science and Engineering, Xinjiang University, China. His research interests include the processing of videos and images under special weather conditions.